to the kinetic isotope effect for the intracomplex proton-transfer reaction.

Acknowledgment. I am grateful to Dr. David F. Eaton for suggesting this research problem and for his critical reading of the manuscript and useful discussions. Drs. T. Dueber, A. Anderson, and B. Monroe kindly supplied the sample dyes used in this work. I thank Dr. J. B. Kinney for developing software for the single proton counting instrument, E. Mathew for obtaining some of the absorption and fluorescence spectral data, and G. Reddy for performing 2D NOE experiment. The technical assistance of Ms. S. Harvey is also appreciated.

Registry No. DBI, 5706-20-7; JDI, 72700-01-7.

UV Resonance Raman Studies of Acetone, Acetamide, and *N*-Methylacetamide: Models for the Peptide Bond

John M. Dudik, Craig R. Johnson, and Sanford A. Asher*

Department of Chemistry, University of Pittsburgh, Pittsburgh, Pennsylvania 15260
(Received: December 17, 1984; In Final Form: May 7, 1985)

The UV Raman excitation profiles of acetone, acetamide, and *N*-methylacetamide have been measured between 217 and 560 nm. No enhancement is observed from the weak $n \rightarrow \pi^*$ transitions of these compounds. The preresonance enhancement of acetone vibrations appears to derive from transitions in the far-UV. The carbonyl stretch shows more preresonance enhancement than the C–C stretching vibrations. The preresonance enhancement of acetamide and *N*-methylacetamide vibrations derives primarily from the $\pi \rightarrow \pi^*$ transitions located at 182 and 188 nm, respectively. Those amide vibrations which have large contributions of C–C stretching or methyl group deformation show more preresonance enhancement from UV transitions at energies higher than the $\pi \rightarrow \pi^*$ transition. It may be possible to selectively enhance protein amide vibrational modes with UV excitation within the ca. 180-nm $\pi \rightarrow \pi^*$ transitions.

Introduction

The increased use of Raman and resonance Raman spectroscopy for molecular structural studies,[1] especially biophysical studies,[2-4] is primarily due to an increased awareness of the molecular information available from complex systems from Raman spectral measurements. Resonance Raman spectroscopy is of major utility in biophysical studies because of its selectivity and its high sensitivity. This selectivity has been of decisive advantage in studies of biomolecules such as visual pigments[5] and heme proteins.[6-8] Resonance Raman spectroscopy has also recently found utility in the examination of electronic excited states;[9-11] the vibrational modes which are resonance enhanced depend upon the electron density changes and geometric alterations between the ground and excited states involved in the resonant transition.[12] Thus, the enhancement pattern can be used to assign the absorption bands, and also can be used to examine geometric changes between the ground and excited states.[13-15]

Recently our laboratory began studies of resonance Raman enhancement in the UV spectral region (220–400 nm).[16] We examined preresonance enhancement and measured the Raman cross sections[17] of simple molecules such as CH_3CN, ClO_4^-, NO_3^-, and SO_4^{2-}; these species are useful internal intensity standards. We also examined resonance enhancement in benzene,[18] polycyclic aromatic hydrocarbons such as naphthalene and pyrene,[19-21] aromatic amino acids,[22] and proteins.[22] Recently, other workers have used excitation further in the UV, below 220 nm, to study substituted benzenes,[23,24] ethylene,[25] ammonia,[26] aromatic amino acids,[27] and, more recently, *N*-methylacetamide.[28]

In this report we examine the UV preresonance enhancement of the vibrations of acetone, acetamide, and *N*-methylacetamide to determine which excited electronic states are responsible for the preresonance Raman intensities. We find that the preresonance enhancements of the amide vibrations derive almost entirely from the lowest energy $\pi \rightarrow \pi^*$ transitions at ca. 180 nm. Direct excitation into these absorption bands in protein and peptide samples may result in a strong, selective enhancement of those amide vibrational modes which have already been shown by normal Raman spectroscopy[2-4] to report directly on protein secondary structure.

Experimental Section

The tunable UV Raman spectrometer used in these studies has been described in detail elsewhere.[16] The acetone solutions were recirculated through a jet nozzle having a rectangular orifice of 0.2 × 3 mm. To avoid acetone evaporation, a 4.5-cm-long Suprasil tube (i.d. 2.5 cm) enclosed the jet nozzle. A heating coil, wrapped around the outside of the Suprasil tube, prevented acetone con-

(1) Long, D. A. "Raman Spectroscopy"; McGraw-Hill: New York, 1977.
(2) Carey, P. R. "Biochemical Applications of Raman and Resonance Raman Spectroscopies"; Academic Press: New York, 1982.
(3) Tu, A. T. "Raman Spectroscopy in Biology: Principals and Applications"; Wiley: New York, 1982.
(4) Parker, F. S. "Applications of Infrared, Raman, and Resonance Raman Spectroscopy in Biochemistry"; Plenum Press: New York, 1983.
(5) Mathies, R. In "Chemical and Biochemical Applications of Lasers"; Moore, C. B., Ed.; Academic Press: New York, 1979; p 55.
(6) Asher, S. A. *Methods Enzymol* **1981**, *76*, 371.
(7) Rousseau, D. L.; Friedman, J. M.; Williams, P. T. *Top. Curr Phys.* **1979**, *2*, 203.
(8) Spiro, T. G. In "Iron Porphyrins, Part II"; Lever, A. B. P., Gray, H. B., Eds.; Addison-Wesley: Reading, MA, 1983; p 89.
(9) Clark, R. J. H.; Stewart, B. *Struct. Bonding (Berlin)* **1979**, *36*, 1.
(10) Asher, S. A.; Sauer, K. *J. Chem. Phys.* **1976**, *64*, 4115.
(11) Hirakawa, A. Y.; Tsuboi, M. In "Vibrational Spectra and Structure"; Durig, J. R., Ed.; Elsevier: New York, 1983; p 145.
(12) Siebrand, W.; Zgierski, M. Z. "Excited States IV"; Academic Press: New York, 1979; p 1.
(13) Peticolas, W. L.; Blazej, D. C. *Chem. Phys. Lett.* **1979**, *63*, 604.
(14) Suzubi, E.; Homoguchi, H.; Harada, I.; Matsuura, H.; Shimanouchi, R. *J. Raman Spectrosc.* **1976**, *4*, 91.
(15) Jones, C. M.; Johnson, C. R.; Asher, S. A.; Shepherd, R. E. *J. Am. Chem. Soc.* **1985**, *107*, 3772.
(16) Asher, S. A.; Johnson, C. R.; Murtaugh, J. *Rev. Sci. Instrum.* **1983**, *54*, 1657.
(17) Dudik, J. M.; Johnson, C. R.; Asher, S. A. *J. Chem. Phys.* **1985**, *82*, 1732.
(18) Asher, S. A.; Johnson, C. R. *J. Phys. Chem.* **1985**, *89*, 1375.
(19) Asher, S. A. *Anal. Chem.* **1984**, *56*, 720.
(20) Asher, S. A.; Johnson, C. R. *Science* **1984**, *225*, 311.
(21) Johnson, C. R.; Asher, S. A. *Anal. Chem.* **1984**, *56*, 2258.
(22) Johnson, C. R.; Ludwig, M.; O'Donnell, S. E.; Asher, S. A. *J. Am. Chem. Soc.* **1984**, *106*, 5008.
(23) Ziegler, L. D.; Hudson, B. *J. Chem. Phys.* **1981**, *74*, 982.
(24) Ziegler, L. D.; Hudson, B. *J. Chem. Phys.* **1983**, *79*, 1134.
(25) Ziegler, L. D.; Hudson, B. *J. Chem. Phys.* **1983**, *79*, 1197.
(26) Zeigler, L. D.; Hudson, B. *J. Phys. Chem.* **1984**, *88*, 1100.
(27) Rava, R. P.; Spiro, T. G. *J. Am. Chem. Soc.* **1984**, *106*, 4062.
(28) Mayne, L. C.; Ziegler, L. D.; Hudson, B. *J. Phys. Chem.*, submitted.

0022-3654/85/2089-3805$01.50/0

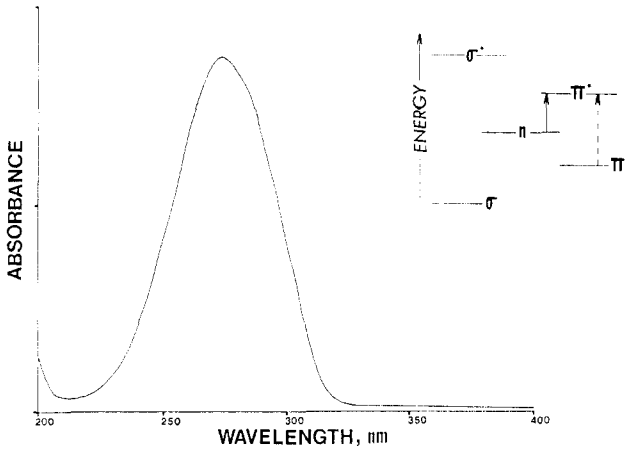

Figure 1. UV absorption spectrum of acetone in CH_3CN.

densation on the inner wall. Equilibrium between the liquid and gas phases of acetone was established after 4 min of recirculation; a 15% loss in acetone concentration was typically observed for the liquid solution. Absorption spectral measurements indicated that after equilibrium was established the concentration of acetone remained essentially constant during the time interval of the spectral measurement. Fresh samples of acetone, acetamide, and *N*-methylacetamide were used for each spectrum measured for the excitation profiles. The amide solutions were recirculated through the laser beam through a Suprasil quartz capillary by a peristaltic pump.

The laser beam was focused above the sample solutions to avoid nonlinear effects. Absorption spectra of all solutions were obtained before and after each spectral measurement to check for concentration changes or sample photochemical decomposition. The monochromator throughput efficiency was calibrated in the visible region with a standard intensity incandescent lamp and in the UV region with a standard intensity deuterium lamp. The output of the standard intensity lamp was scattered from a Lambert surface prepared with Eastman Kodak white reflectance standard and imaged into the monochromator with the Raman collection optics. Acetone and acetonitrile were obtained from the J. T. Baker Co. and Burdick and Jackson, respectively. Acetamide and *N*-methylacetamide were obtained from the Aldrich Chemical Co.

The relative intensity values used in the excitation profiles were determined from peak height measurements of the Raman bands. The analyte Raman intensities were referenced to an internal intensity standard; the 918-cm^{-1} peak (C–C stretching vibration) of the acetonitrile solvent was used as the internal intensity standard for the acetone studies, while the 932-cm^{-1} (symmetric stretch) of perchlorate was used for the acetamide studies. We recently determined the dispersion of the absolute Raman cross sections of these intensity standards[17] from 217 to 640 nm and have corrected the excitation profile data for the wavelength dependence of the internal standard Raman cross sections. We estimate that the Raman frequencies quoted are accurate to ±5 cm^{-1}.

Results

The absorption spectrum of acetone in the near-UV spectral region and an energy level diagram which depicts the electronic transitions of acetone are shown in Figure 1. The only feature observed in the UV–visible absorption spectrum between 200 and 600 nm is the broad forbidden n → π* absorption band at 275 nm. The molar absorptivity of this band is low (~15 L/(mol·cm)). Raman spectra obtained by exciting through the n → π* region are displayed in Figure 2. The dominant features in the spectra are due to acetonitrile. The peaks labeled with an S at 380, 918, and 1376 cm^{-1} derive from acetonitrile.[29] The three most intense vibrational modes of acetone[30] are the symmetric C–C stretch at

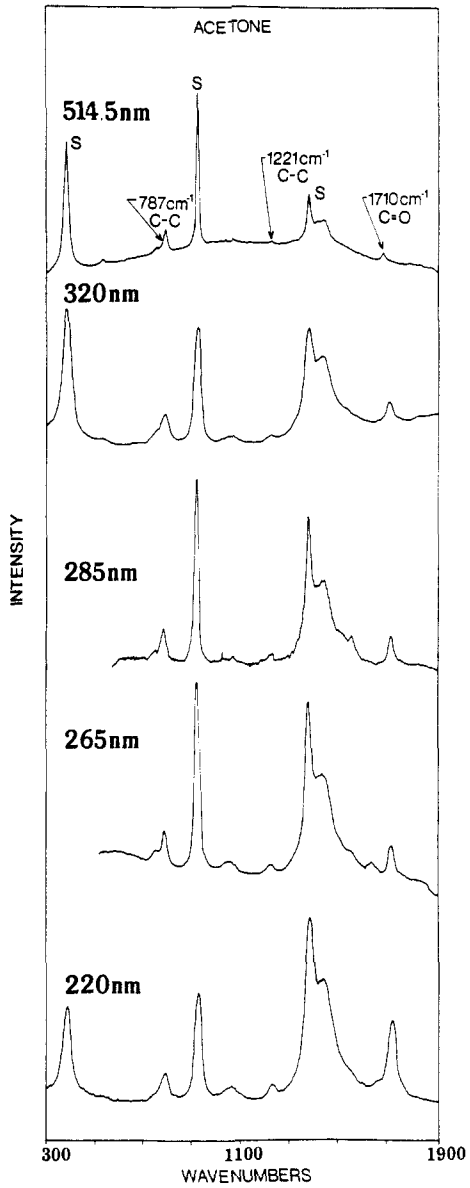

Figure 2. Raman spectra of a 1.3 M solution of acetone in acetonitrile excited at 514.5, 320, 285, 265, and 220 nm. The acetonitrile peaks are labeled with an S. The 514.5-nm spectrum was accumulated over 2 min with a laser power of 0.7 W. Spectral resolution is ca. 5 cm^{-1}. The 320- and 220-nm spectra were obtained with laser pulse energies of 2.0 and 0.8 mJ, respectively. The spectra were accumulated in 10 min at a 20-Hz laser pulse repetition rate. The spectral resolution is ca. 28 cm^{-1}. The 285- and 265-nm spectra were obtained in a 15-min accumulation with a 1.0-mJ laser pulse energy. The spectral resolution for the spectra excited at 285 and 265 nm is ca. 18 cm^{-1}.

787 cm^{-1}, the asymmetric C–C stretch at 1221 cm^{-1}, and the C=O stretch at 1710 cm^{-1}. The top spectrum in Figure 2 was obtained with preresonance excitation at 514.5 nm, the middle three spectra were obtained with excitation in resonance with the n → π* absorption band, and the bottom spectrum was obtained with 220-nm excitation at an energy above the n → π* transition.

The spectra in Figure 2 show no indication of resonance enhancement from the forbidden n → π* transition of acetone since none of the acetone bands display any dramatic increase or decrease in intensity compared to the acetonitrile peaks. This is expected since the Raman cross section is proportional to the magnitude (to some power >1) of the oscillator strength of the resonant transition; the low molar absorptivity value (~15 L/(mol·cm)) of the n → π* band of acetone should result in little or no resonance enhancement from this transition.

(29) Herzberg, G. "Infrared and Raman Spectra of Polyatomic Molecules"; Van Nostrand: New York, 1945; p 333.

(30) Cleveland, F. F.; Murray, M. J.; Coley, J. R.; Komarewsky, V. I. *J. Chem. Phys.* **1942**, *10*, 18.

TABLE I: Total Differential Raman Cross Sections

	$\sigma_R \times 10^{-30}$ cm²/(mol·sr)		$\sigma_{220}/\sigma_{514.5}$
	514.4 nm	220 nm	
	Acetone[a]		
1710 cm⁻¹, C=O	0.6	370	620
1221 cm⁻¹, C–C	0.3	60	200
787 cm⁻¹, C–C	2.4	130	54

	$\sigma_R \times 10^{-30}$ cm²/(mol·sr)			
	560 nm	365 nm	220 nm	$\sigma_{220}/\sigma_{560}$
	Acetamide[b]			
1616 cm⁻¹, (amide II)		3.4	700	
1404 cm⁻¹, (amide III)	0.3	3.9	1000	3500
1131 cm⁻¹	1.3[c]	13[c]	320[c]	250
1005 cm⁻¹	0.1	0.4	100	1000
871 cm⁻¹	1.6	13	470	300
	N-Methylacetamide[b]			
1581 cm⁻¹, (amide II)		2.2	2600	
1316 cm⁻¹, (amide III)	0.5	8.2	3900	7800
1162 cm⁻¹	0.4	3.1	280	700
881 cm⁻¹	1.6	13	1100	680
628 cm⁻¹, (amide IV)			380	

[a] The cross sections were determined by using peak height measurements and referencing the intensities to the cross section of the 918-cm⁻¹ CH_3CN vibration.[17] [b] The cross sections were determined by using peak height measurements and referencing the intensities to the cross section of the 932-cm⁻¹ ClO_4^- vibration.[17] [c] The cross sections were determined by using peak area measurements and referencing the intensities to the cross section (peak area) of the 932-cm⁻¹ ClO_4^- vibration.[17]

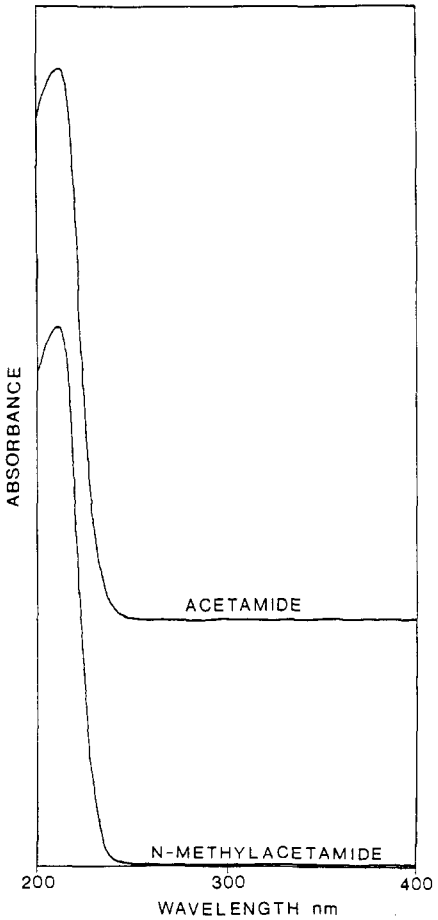

Figure 3. Absorption spectra of aqueous solutions of acetamide and *N*-methylacetamide in the UV.

As the excitation wavelength decreases from 514.5 to 220 nm the intensity of all three acetone bands increase compared to the 918-cm⁻¹ peak of acetonitrile. From our earlier Raman cross section studies[17] we know that the 918-cm⁻¹ peak cross section shows essentially no preresonance enhancement and increases approximately as ν^4. The total differential Raman cross sections of the three vibrations of acetone excited at 220 and 514.5 nm are listed in Table I. The fact that the intensities of the bands of acetone increase at different rates in the preresonance region indicates that differences exist in the contribution of excited states to the preresonance enhancement of the different vibrations.

The UV absorption spectra[31-35] of acetamide and *N*-methylacetamide (Figure 3) show forbidden $n \rightarrow \pi^*$ transitions at ca. 210 nm which have maximum molar absorptivities of ca. ~60 L/(mol·cm). Figures 4 and 5 display the Raman spectra of

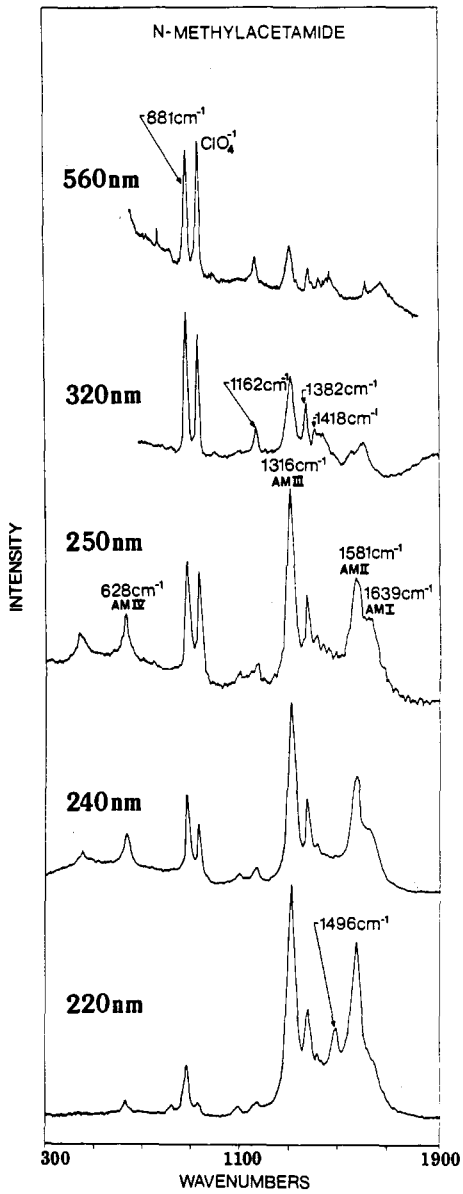

Figure 4. Raman spectra of aqueous solutions of *N*-methylacetamide. The *N*-methylacetamide concentration was 1.0 M for the spectra excited at 560 and 365 nm, and 0.4 M for the spectra excited at 250, 240, 220 nm. The internal standard, perchlorate, is 0.2 M in all solutions. The 560- and 365-nm spectra were accumulated with a 6.0-mJ laser pulse energy in 30 min at 20 Hz. The 250-, 240-, and 220-nm spectra were obtained with laser pulse energies of ca. 0.5 mJ in 15-min scans. The spectral resolution in the 560-, 365-, 250-, 240-, and 220-nm spectra are ca. 5, 11, 6, 6, and 7 cm⁻¹, respectively.

(31) Robin, M. B. "Higher Excited States of Polyatomic Molecules"; Academic Press: New York, 1975; Vol. II.
(32) Basch, H.; Robin, M. B.; Kuebler, N. A. *J. Chem. Phys.* **1968**, *49*, 5007.
(33) Nielsen, E. B.; Schellman, J. A. *J. Phys. Chem.* **1967**, *71*, 2297.
(34) Kaya, K.; Nagakura, S. *Theoret. Chim. Acta* **1967**, *7*, 117.
(35) Basch, H.; Robin, M. B.; Kuebler, N. A. *J. Chem. Phys.* **1967**, *47*, 1201.

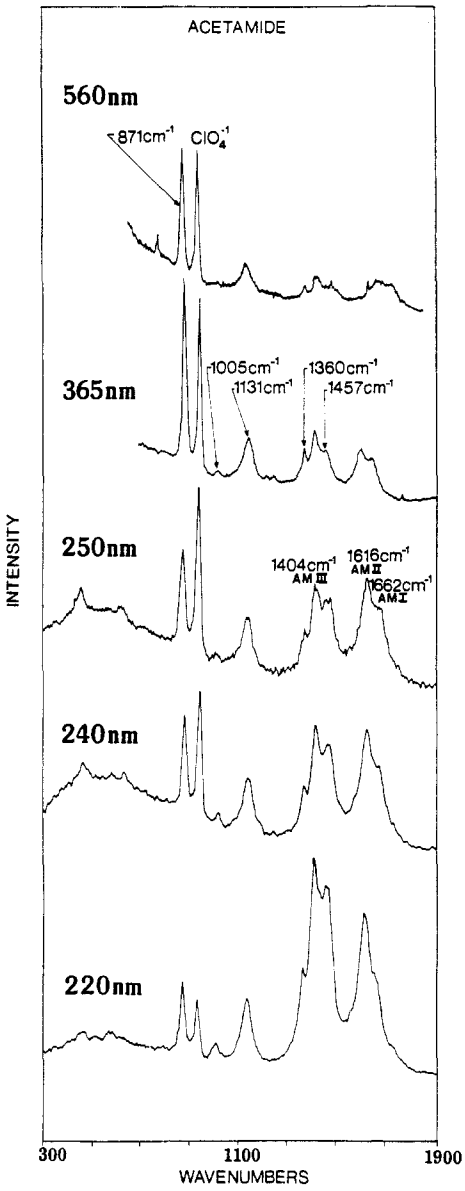

Figure 5. Raman spectra of a 1.0 M solution of acetamide in water excited at 560 and 365 nm, and a 0.4 M solution excited at 250, 240, and 220 nm. The perchlorate is 0.2 M in all solutions. The experimental parameters are the same as for *N*-methylacetamide (Figure 4).

aqueous solutions of *N*-methylacetamide and acetamide obtained with excitation at 560, 365, 250, 240, and 220 nm. The in-plane vibrations known as the amide I to IV bands are labeled with "AM" in the figures. The amide I bands located at 1639 cm^{-1} in *N*-methylacetamide[28,36-39] and at 1662 cm^{-1} in acetamide[40,41] originate primarily from C=O stretching and are most evident with 560-nm excitation. For *N*-methylacetamide the amide II band occurs at 1581 cm^{-1} and results from a combination of NH bending and C–N stretching, whereas for acetamide an amide II-like band occurs at 1616 cm^{-1} and is associated with NH_2 bending and contains a small contribution from C=O stretching. The *N*-methylacetamide amide III band is located at 1316 cm^{-1} and derives from C–N stretching, NH in-plane bending, NCO bending, and C–C stretching. The amide III-like band of acetamide, located at 1404 cm^{-1}, contains a large contribution from C–N stretching, as well as minor contributions from C–C stretching, NH_2 rocking, and symmetric deformations of the NCO group and CH_3 groups. The amide IV band occurs at 628 cm^{-1} in *N*-methylacetamide and originates from a combination of C–C stretching and NCO bending.

The observed vibrations of *N*-methylacetamide[28,36-39] also include a C–C stretching and NCO bending vibration at 881 cm^{-1}, a N–CH_3 rocking vibration at 1162 cm^{-1}, a symmetric bend of the C–CH_3 group at 1382 cm^{-1}, and a symmetric bend of the N–CH_3 group at 1418 cm^{-1}. The 1496-cm^{-1} band arises from asymmetric bends of both CH_3 groups. The peak located at 932 cm^{-1} is from the internal standard, perchlorate. The broad H–O–H bending vibration of water, the solvent, contributes to the Raman intensity around 1600 cm^{-1}.

Other Raman active vibrations of acetamide[40,41] include a band at 871 cm^{-1} which has a large contribution from C–C stretching and a minor contribution from C–N stretching. The 1005-cm^{-1} vibration results from CH_3 rocking and asymmetric deformation. The band at 1131 cm^{-1} derives from NH_2 rocking motion and C=O stretching, and the bands at 1360 and 1457 cm^{-1} result from symmetric and asymmetric deformations of the CH_3 group.

The spectra in Figures 4 and 5 show that as the excitation wavelength decreases from 560 to 220 nm all the Raman peaks increase in intensity relative to perchlorate. The vibrations of *N*-methylacetamide show a larger intensity increase than those of acetamide. This suggests that the energy of the preresonant state giving rise to the Raman enhancement in *N*-methylacetamide is lower than that in acetamide. The total differential Raman cross sections of the vibrations of acetamide and *N*-methylacetamide excited at 560, 365, and 220 nm are displayed in Table I. For both compounds the amide I, II, and III bands display the largest intensity increase. Indeed, the amide II bands of acetamide and *N*-methylacetamide are very weak and barely observable with visible excitation. Harada et al.[36] previously observed selective preresonance enhancement for this band with excitation at 257.3 nm in *N*-methylacetamide, *N*-ethylacetamide, and *N*-methylpropionamide. Mayne et al.[28] recently demonstrated much larger enhancements of amide bands in *N*-methylacetamide with excitation below 218 nm.

Discussion

The total Raman scattering cross section, σ_{mn}, for a vibrational transition n ← m integrated over 4π sr for an isolated molecule averaged over all orientations is[17,42,43]

$$\sigma_{mn} = \frac{I_{mn}}{I_0} = \frac{2^7\pi^5}{3^2}\nu_0(\nu_0 - \nu_{mn})^3 g f(T) \sum_{\rho\sigma} |\alpha_{\rho\sigma}(\nu_0)|^2 \qquad (1)$$

I_{mn} is the Raman intensity integrated over 4π sr over the bandwidth of the vibrational transition n ← m. I_0 is the intensity of the incident laser beam. ν_0 and ν_{mn} are the energies (cm^{-1}) of the excitation beam and vibrational transition, respectively. The factor $\nu_0(\nu_0 - \nu_{mn})^3$ is used instead of the commonly seen $(\nu_0 - \nu_{mn})^4$ factor because I_{mn} is in units of photons/(s·cm^2). g is a factor specifying the degeneracy of the initial state, m, and $f(T)$ is the Boltzmann weighting factor describing the thermal occupancy of the initial state. $\alpha_{\rho\sigma}(\nu_0)$ is the ρ,σth component (ρ,σ = x,y,z) of the Raman polarizability tensor for excitation at ν_0.

The differential Raman scattering cross section, σ_R, for 90° collection of both the parallel and perpendicular polarized scattering from a molecule in a solution where the incident beam is polarized perpendicular to the scattering plane is[17,42,43]

$$\sigma_R = \frac{d\sigma_{mn}(\nu_0)}{d\Omega} = \frac{2^4\pi^4}{45}\nu_0(\nu_0 - \nu_{mn})^3 g f(T) b^2 L(45\alpha^2 + 7\gamma^2) \qquad (2)$$

b is the zero point vibrational amplitude which is equal to $(h/8\pi c^2\nu_{mn})^{1/2}$. α^2 is the isotropic and γ^2 is the anisotropic invariant of the polarizability tensor. L is the local field correction which

(36) Harada, I.; Sugawara, Y.; Matsuura, H.; Shimanouchi, T. *J. Raman Spectrosc.* **1975**, *4*, 91.
(37) Jakes, J.; Schneider, B. *Collect. Czech. Chem. Commun.* **1968**, *33*, 643.
(38) Schneider, B.; Horeni, A.; Picova, H.; Honzi, J. *Collect. Czech. Chem. Commun.* **1965**, *30*, 2196.
(39) Miyazawa, T.; Shimanouchi, T.; Mizushima, S.-I. *J. Chem. Phys.* **1958**, *29*, 611.
(40) Uno, T.; Machida, K.; Saito, Y. *Bull. Chem. Soc. Jpn.* **1969**, *42*, 897; *Spectrochim Acta, Part A* **1971**, *27A*, 833.
(41) Suzuki, I. *Bull. Chem. Soc. Jpn.* **1962**, *35*, 1279.
(42) Schrotter, H. W.; Klockner, H. W. In "Topics in Current Physics"; Weber, A., Ed.; Springer-Verlag: West Berlin, 1979; p 123.
(43) Eckhardt, G.; Wagner, W. G. *J. Mol. Spectrosc.* **1966**, *19*, 407.
(44) Abe, N.; Wakayama, M.; Ito, M. *J. Raman Spectrosc.* **1977**, *6*, 38.

TABLE II: Comparison between the Excited-State Energies Determined by Nonlinear Least Squares Fits to the A Term ($K_2 \equiv 0$) and Modified A-term Expressions for Acetone, Acetamide, and *N*-Methylacetamide

	A term[a]		modified A term[b]			
mode, cm^{-1}	$\nu_e \times 10^3$, cm^{-1}	$K_1 \times 10^{16}$, cm^{-1} molecule^{-1} sr^{-1}	$\nu_e \times 10^3$, cm^{-1}	$K_1 \times 10^{16}$, cm^{-2} molecule^{-1} sr^{-1}	$K_2 \times 10^{-9}$, cm	% change in residual sum of squares[c]
			Acetone			
1710 (C=O)	79.7 (2.7)[d] (126 ± 9)[e]	236	57.0 (3.2) (176 ± 22)	1.10	3.12	32
1221 (C=C)	111.0 (11.2) (90 ± 20)	524	68.2 (28.9) (~150)	1.68	1.41	0
787 (C-C)	153.0 (22.6) (65 ± 25)	8970	54.2 (8.2) (184 ± 80)	0.275	26.6	18
			Acetamide			
1616 (amide II)	59.0 (1.4) (170 ± 10)	49.2	58.7 (4.9) (170 ± 35)	44.2	0.042	2
1404 (amide III)	55.8 (0.8) (179 ± 6)	24.4	55.8 (2.3) (179 ± 18)	24.0	8×10^{-7}	0
1131	59.5 (1.2) (168 ± 8)	27.3	57.3 (2.7) (174 ± 20)	11.3	0.418	9
1005	53.5 (0.3) (187 ± 3)	1.2	53.0 (0.8) (189 ± 6)	0.845	0.412	6
871	68.7 (0.6) (146 ± 3)	269	57.5 (1.8) (174 ± 12)	9.60	1.65	42
			N-Methylacetamide			
1581 (amide II)	53.5 (1.3) (187 ± 10)	20.9	53.3 (3.9) (188 ± 35)	19.2	5×10^{-7}	0
1316 (amide III)	54.6 (1.4) (183 ± 11)	53.0	54.4 (4.2) (184 ± 35)	48.7	5×10^{-8}	0
1162	56.8 (1.7) (176 ± 12)	8.7	51.2 (1.2) (195 ± 10)	0.340	5.38	69
881	59.0 (2.6) (170 ± 18)	77.5	56.9 (5.9) (176 ± 50)	32.6	0.453	2
628 (amide IV)	58.3 (2.3) (172 ± 16)	22.0	52.4 (2.5) (191 ± 22)	0.894	4.81	38

[a] Equation 5 with $K_2 \equiv 0$. [b] Equation 5. [c] % decrease in the residual sum of squares from the A-term fit to the modified A-term fit. [d] Standard error of the coefficient is indicated in parentheses. [e] Approximate 95% confidence limits are indicated for the wavelength of the excited state in nanometers.

accounts for the increased electric field amplitude in the condensed-phase sample over that which would occur in the gas phase and is

$$L = (n_s/n_0)(n_s^2 + 2)^2(n_0^2 + 2)^2/81$$

where n_s and n_0 are the sample refractive indices at $(\nu_0 - \nu_{mn})$ and ν_0, respectively.

The Raman scattering cross section is obtained by measuring the ratio of the analyte scattered Raman intensity (I_A) to the internal standard Raman intensity (I_S) and multiplying this ratio by the known Raman scattering cross section of the internal standard,[17] $\sigma_S(\nu_0)$:

$$\frac{\sigma_A(\nu_0)}{\sigma_S(\nu_0)} = \frac{I_A}{I_S}\frac{E(\nu_0 - \nu_S)}{E(\nu_0 - \nu_A)}\frac{C_S}{C_A} = \frac{(\nu_0 - \nu_A)^3}{(\nu_0 - \nu_S)^3}\frac{(45\alpha^2 + 7\gamma^2)_A}{(45\alpha^2 + 7\gamma^2)_S} \quad (3)$$

$E(\nu_0 - \nu_S)$ and $E(\nu_0 - \nu_A)$ are the spectrometer throughput efficiencies for the collected Raman scattered light of the internal standard and analyte, respectively. The factor C_S/C_A corrects for the concentration difference between the internal standard and analyte. Defining the parameter $S = (45\alpha^2 + 7\gamma^2)$, which we call the relative scattering power, we relate the observed relative Raman intensities to relative scattering powers; S monitors the excitation frequency dependence of the modulus squared of the Raman polarizability tensor elements.

$$S_A = \frac{I_A}{I_S}\frac{E(\nu_0 - \nu_S)}{E(\nu_0 - \nu_A)}\frac{C_S}{C_A}\frac{(\nu_0 - \nu_S)^3}{(\nu_0 - \nu_A)^3}S_S \quad (4)$$

S_S is the scattering power of the internal standard, which we determined previously[17] in our cross section measurements of CH_3CN and ClO_4^-. Thus, the preresonance excitation profiles detail the excitation frequency dependence of the Raman polarizability tensor elements.

The excitation profile data obtained by using eq 4 for various modes of acetone, acetamide, and *N*-methylacetamide are shown in Figures 6–8. The abscissa is the relative scattering power (arbitrary scales). The solid lines in Figures 6A–8A result from nonlinear least-squares fits of the data to an Albrecht A-term expression.[45] The A-term model assumes that only a single, dipole-allowed electronic transition contributes to the preresonance Raman enhancement:

$$S_A = K_1\left[\frac{\nu_e^2 + \nu_0^2}{(\nu_e^2 - \nu_0^2)^2} + K_2\right]^2 \quad (5)$$

where $K_2 \equiv 0$ is an A-term fit and $K_2 \neq 0$ is a modified A-term fit. K_1 is a constant independent of excitation energy and depends upon the oscillator strength of the transition and the coupling between the vibration and the electronic transition. ν_0 is the excitation energy (cm^{-1}), and ν_e is the energy (cm^{-1}) of the resonant excited state. The solid lines in Figures 6B–8B derive from nonlinear least-squares fits of the data to a modified A term given by eq 5 when $K_2 \neq 0$. We have recently shown[17,18] in studies of benzene, CH_3CN, SO_4^{2-}, ClO_4^-, and NO_3^- that this modification of the standard A-term results in more physically reasonable transition energies and may help pick out the contribution of discrete low-lying preresonant excited states. The K_2 parameter in the modified A-term models the contribution of all important far-UV states as if they were at infinite energy. Phenomenologically, separating out the contribution of the higher energy transitions results in a decrease in the calculated energy (ν_e) of the preresonant excited state. When the K_2 term is important a noticeable improvement (vide infra) in the fit is seen when compared to the standard A term ($K_2 = 0$), particularly for the low-energy excitation profile data where the K_2 term may dominate. The parameters obtained for the standard and modified A-term nonlinear least-squares fits are shown in Table II. The nonlinear curve-fitting procedure used to determine the parameters is based on the "maximum neighborhood" method.[46a,c] The criterion for convergence in the fit is when the residual sum of squares changes by less than 1×10^{-6} between successive iterations. Similar results were obtained with a program based on the "gradient expansion" method,[46b] but convergence was slower.

The A-term fits shown in Figure 6A demonstrate that no resonance enhancement derives from the ca. 36 000-cm^{-1} $n \rightarrow \pi^*$ band of acetone. The C–C stretches at 787 and 1221 cm^{-1} show a slight preresonance enhancement at higher excitation energies. In contrast, the C=O stretch shows a greater preresonance enhancement. This indicates that the C=O stretch derives more preresonance enhancement from electronic transitions occurring lower in energy than in electronic transitions responsible for the slight preresonance enhancements of the C–C stretches.

The A-term fit indicates a preresonant state for the C=O stretch at 80 000 cm^{-1} (125 nm). In contrast, the 787- and 1221-cm^{-1} C–C symmetric and asymmetric stretches show

(45) Albrecht, A. C.; Hutley, M. C. *J. Chem. Phys.* **1971**, *55*, 4438.

(46) (a) Daniel, C.; Wood, F. S. "Fitting Equations to Data"; Wiley-Interscience: New York, 1971. (b) Bevington, P. R. "Data Reduction and Error Analysis for the Physical Sciences"; McGraw-Hill: New York, 1969. (c) Program NONLINWOOD available from the Share Program Library Agency, Triangle Universities Computation Center, Box 12076, Research Triangle Park, NC 27709; Program No. 360D-13.6007.

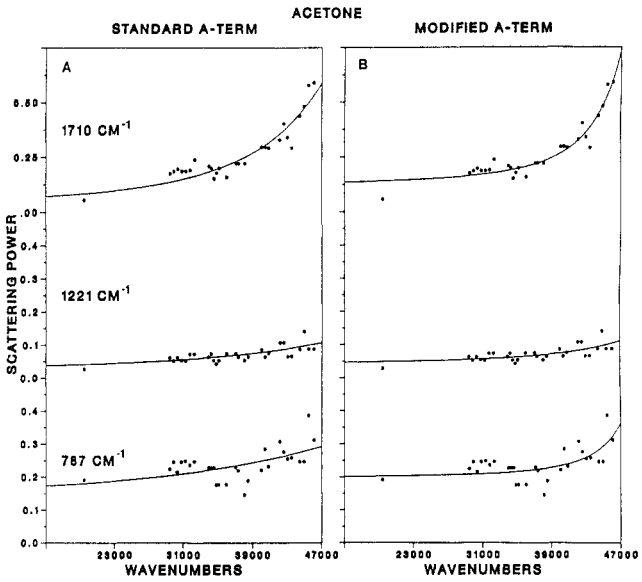

Figure 6. Raman excitation profiles of acetone. The ordinate is the scattering strength (arbitrary units). The lines connecting the data derive from an Albrecht A-term nonlinear least-squares best fit to eq 5, $K \equiv 0$ (A) and eq 5, $K \neq 0$ (B). See text for details. The ordinate for each profile is independently and arbitrarily scaled.

preresonant states at ca. 153 000 cm^{-1} (65 nm) and 111 000 cm^{-1} (90 nm). These preresonant state energies are higher than the likely energy of the carbonyl $\pi \rightarrow \pi^*$ transition.[31] Strong dipole-allowed transitions occur at energies less than 80 000 cm^{-1} for the carbonyl functional group of ketones in the *gas phase*.[31] Most of these transitions are thought to be Rydberg in character, and no assignment for the $\pi \rightarrow \pi^*$ transition is available, to our knowledge. In contrast, condensed-phase UV absorption spectra of acetone[31] in *n*-hexane display only a broad absorption at 54 000 cm^{-1} (185 nm) which has a maximum molar absorptivity of ca. 10^3 L/(mol·cm).[40] This absorption feature has been assigned as an $n \rightarrow \sigma^*$ transition. It is unclear to us how one describes electronic transitions in *condensed-phase* acetone samples in the vacuum-UV spectral region where any electronic transition is likely to be a concerted transition which simultaneously involves both acetone and solvent molecules.

Using the modified A-term, the calculated energy of the resonant state for the C=O stretch decreases to 57 000 cm^{-1} (176 nm). The resonant state transition energies of the 787-cm^{-1} C–C symmetric stretch and the 1221-cm^{-1} C–C asymmetric stretch decrease to 68 000 cm^{-1} (150 nm) and 54 000 cm^{-1} (185 nm), respectively.

The modified A-term fits to the 1710- and 787-cm^{-1} data show an improvement in the residual sum of squares over the standard A-term fits and indicate a contribution from an excited state at about 180 nm. As seen from a comparison of parts A and B of Figure 6, the modified A-term does a better job of accounting for the scattering power at the lower and higher excitation energies. The modified A-term fit to the 1221-cm^{-1} data does not reduce the residuals. In fact the 1221-cm^{-1} data show so little curvature relative to the scatter of the data that the fit does not converge to single values for the parameters and the values of the parameters depend upon the initial guess. The modified A-term fits do suggest a contribution from an excited state at ~180 nm (possibly the $n \rightarrow \sigma^*$), but the Raman intensity of the three acetone vibrational modes studied is clearly dominated by far-UV states over the range of excitation energies used in this work. The contribution of the 185-nm state to the scattering power at 217 nm (the shortest wavelength used in this work) is about 5% for the 787-cm^{-1} mode and about 33% for the 1710-cm^{-1} mode. A confirmation of the importance of the state at 185 nm to the Raman intensity and a verification of its assignment will require that the excitation profile data be extended into the vacuum UV.

These results indicate that the broad featureless transition centered at 54 000 cm^{-1} in this condensed-phase sample contributes little to the preresonance Raman intensities. The carbonyl $\pi \rightarrow \pi^*$ transition is expected to strongly contribute to the C=O Raman intensity. It is likely that the lower transition energy found in the A-term fits to the C=O stretching data signals a preferential contribution of the $\pi \rightarrow \pi^*$ transition. Unfortunately, no assignment of this transition is available, even for acetone in the gas phase.

The excitation profiles of the 1616- and 1404-cm^{-1} acetamide amide II and III vibrations, as well as the 871-, 1005-, and 1131-cm^{-1} vibrations, are shown in Figure 7. Figure 8 shows the excitation profiles of the *N*-methylacetamide 1581-, 1316-, and 628-cm^{-1} amide II, III, and IV vibrations and the 881- and 1162-cm^{-1} vibrations. The normal A-term fits (eq 5) with $K_2 \equiv 0$ are shown as solid curves in Figures 7A and 8A while Figures 7B and 8B show the modified A-term fits. The excitation profiles of the acetamide amide I, the acetamide 1360- and 1457-cm^{-1} bands, and the *N*-methylacetamide amide I, the *N*-methylacetamide 1382-, 1418-, and 1496-cm^{-1} bands, are not displayed because it is difficult to reliably determine their Raman intensities due to overlapping bands. These bands, however, are also rapidly increasing in intensity as the excitation energy increases.

Except for the 871- and 628-cm^{-1} bands of acetamide and *N*-methylacetamide, and the 1162-cm^{-1} band of *N*-methylacetamide, the normal A-term fits (eq 5) model the preresonance enhancements well. The use of the modified A term (which has one extra adjustable parameter) results in only a minor decrease in the residual sums of squares for all but the 871-cm^{-1} peak of acetamide and the 1162- and 628-cm^{-1} peaks of *N*-methylacetamide. Indeed, the K_2 values found (Table II) are small except for the 871-, 1162-, and 628-cm^{-1} peaks; the first term in eq 5 (the normal A-term amplitude) would have values of 0.6×10^{-9} and 5×10^{-9} cm^2 for 20 000- and 40 000-cm^{-1} excitation if ν_e = 50 000 cm^{-1}. This signifies that one resonant A-term active excited state gives rise to essentially all of the observed Raman intensity of the amide II and III vibrations of acetamide and *N*-methylacetamide. In contrast, a significant improvement in the fit as judged by a reduction of the residual sum of squares occurs for the 871-cm^{-1} peak of acetamide and the 1162-cm^{-1} peak and 628-cm^{-1} amide IV vibration of *N*-methylacetamide. The larger values found for K_2 clearly indicate the importance of additional states in the far-UV to the Raman intensities (especially for excitation in the visible and near UV spectral region).

The individual contributions of the terms in Figure 5 are more clearly illustrated in Figure 9 where the fits to two of the acetamide modes are shown in detail. Inclusion of the K_2 term produces a large improvement in the 871-cm^{-1} fit but only mildly effects the fit for the 1131-cm^{-1} mode. For the 871-cm^{-1} mode the K_2 term dominates until the excitation energy exceeds ~29 000 cm^{-1}. The K_2 term will always contribute the most at the lowest excitation energies. The A term dominates as the excitation energy approaches the preresonant excited state. At intermediate excitation energies the cross term $2K_2[\nu_e^2 + \nu_o^2/(\nu_e^2 - \nu_o^2)^2]$ provides the largest contribution to the scattering power. Only a constructive interference between the far-UV states and the lower energy state, ν_e, has been assumed. For the 1131-cm^{-1} mode the K_2 term never dominates the scattering power and the A term is predominate for excitation energies above 34 200 cm^{-1}. As with the 871-cm^{-1} mode, however, the K_2 term and cross term contribute to the intensity for the lowest excitation frequencies. In general the data indicate that a single preresonant excited state at ca. 55 000 cm^{-1} is responsible for most of the Raman intensity for all of the modes of acetamide and *N*-methylacetamide.

A similar behavior was observed for the symmetric stretch of NO_3^- where the isolated $\pi \rightarrow \pi^*$ transition at ca. 190 nm was found to be responsible for essentially all of the preresonance enhancement.[17] Some contribution from higher energy excited states does seem indicated, however, for the acetamide 871-, 1131-, and 1005-cm^{-1} modes and the *N*-methylacetamide 1162-, 628-, and 881-cm^{-1} modes. These modes have more single-bond stretching character than the amide II or III modes.

The A-term excited-state energies (Table II) calculated for *N*-methylacetamide are generally 2000–5000 cm^{-1} lower in energy

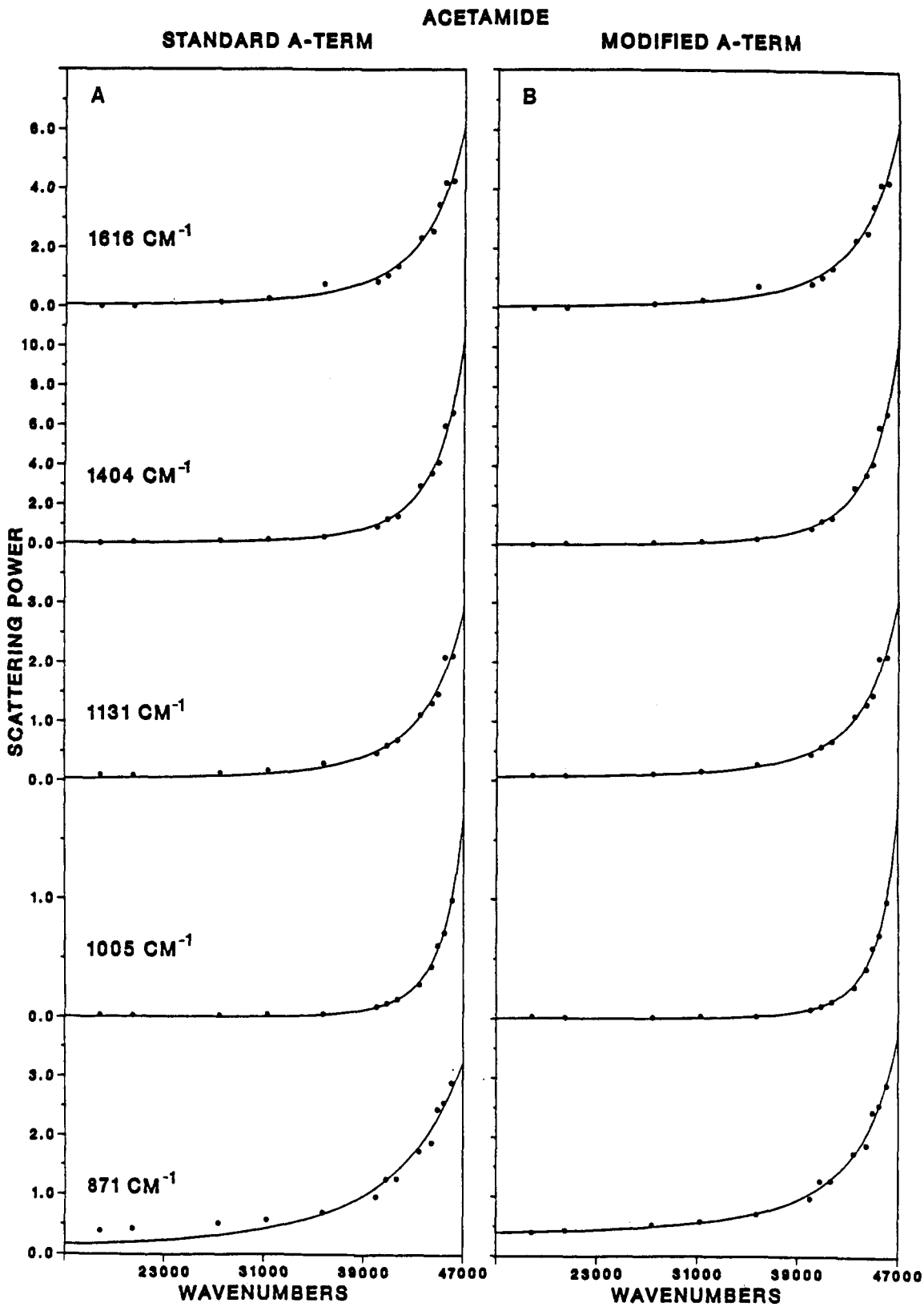

Figure 7. Preresonance Raman excitation profiles of acetamide. The ordinate is the scattering strength (arbitrary units). See text for details. The solid lines correspond to nonlinear least-squares best fits to eq 5, $K \equiv 0$ (A) and eq 5, $K \neq 0$ (B). The ordinate for each profile is independently and arbitrarily scaled.

than those of acetamide. For example, the amide II transition energy in acetamide which occurs at ca. 59 000 cm^{-1} (170 nm) shifts to 53 000 cm^{-1} (188 nm) in *N*-methylacetamide. A similar but smaller shift occurs for the amide III vibration.

UV absorption spectra of condensed- and gas-phase acetamide and *N*-methylacetamide samples show numerous transitions.[31-35] The lowest energy transition is the weak n $\rightarrow \pi^*$ transition at ca. 48 000 cm^{-1} (210 nm) which is shown in Figure 3. A Rydberg n $\rightarrow$ 3s transition occurs at ca. 52 000 (192 nm), while a strong $\pi \rightarrow \pi^*$ transition with $\epsilon \sim 10^4$ L/(mol·cm) occurs between 51–60 000 cm^{-1} (167–196 nm); in H_2O the $\pi \rightarrow \pi^*$ transition of acetamide occurs at 54 900 cm^{-1} (182 nm), but shifts 1600 cm^{-1} to 53 300 (188 nm) in *N*-methylacetamide.[35] The A-term transition energies are very close to the measured energies of the amide $\pi \rightarrow \pi^*$ transitions, and indeed, the decrease in the calculated preresonant state energy of *N*-methylacetamide compared to

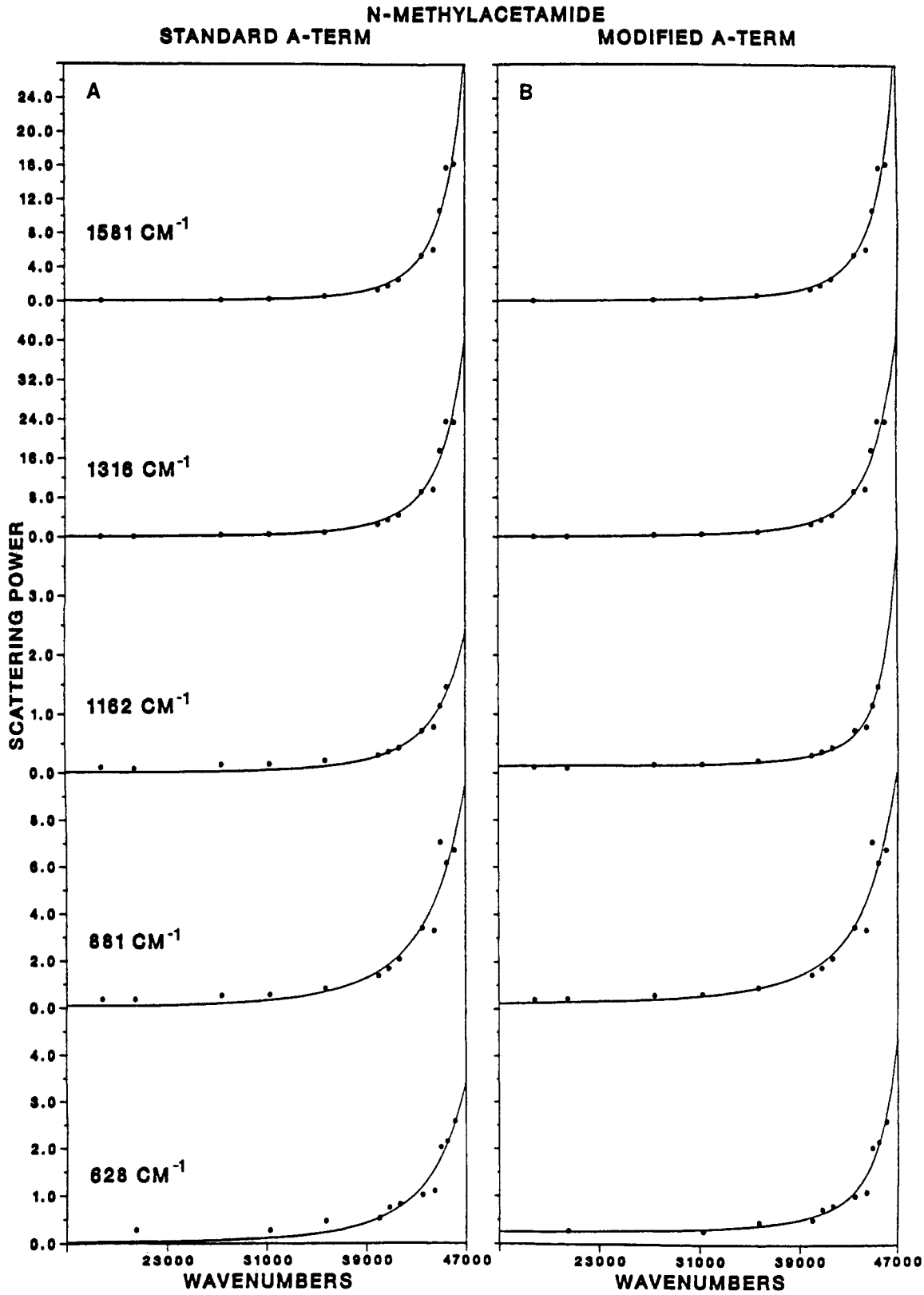

Figure 8. Preresonance Raman excitation profiles of *N*-methylacetamide. The ordinate is the scattering strength (arbitrary units). See text for details. The solid lines correspond to nonlinear least-squares best fits to eq 5, $K \equiv 0$ (A) and eq 5, $K \neq 0$ (B). The ordinate for each profile is independently and arbitrarily scaled.

acetamide is consistent with the absorption spectral shifts.

The dominance of the amide $\pi \rightarrow \pi^*$ transition in the Raman intensities is clearly evident from the close agreement between the A-term transition energies calculated by using either the standard or modified A-term transition expressions. Only the 871-cm^{-1} band of acetamide and the amide IV and 1162-cm^{-1} bands of *N*-methylacetamide show large differences between the transition energies calculated by using the standard or modified A terms. All of the vibrations studied, with the exception of the unique ca. 880-cm^{-1} bands and the *N*-methylacetamide amide IV and 1162-cm^{-1} bands, are dominated by NCO stretching and deformations.[28,36-41] These nuclear motions are expected to strongly couple to the $\pi \rightarrow \pi^*$ transition. In contrast, the unique bands contain significant contributions from C–C stretching and CH_3 rocking which should be less enhanced by the $\pi \rightarrow \pi^*$ transition and could be more enhanced by other transitions at

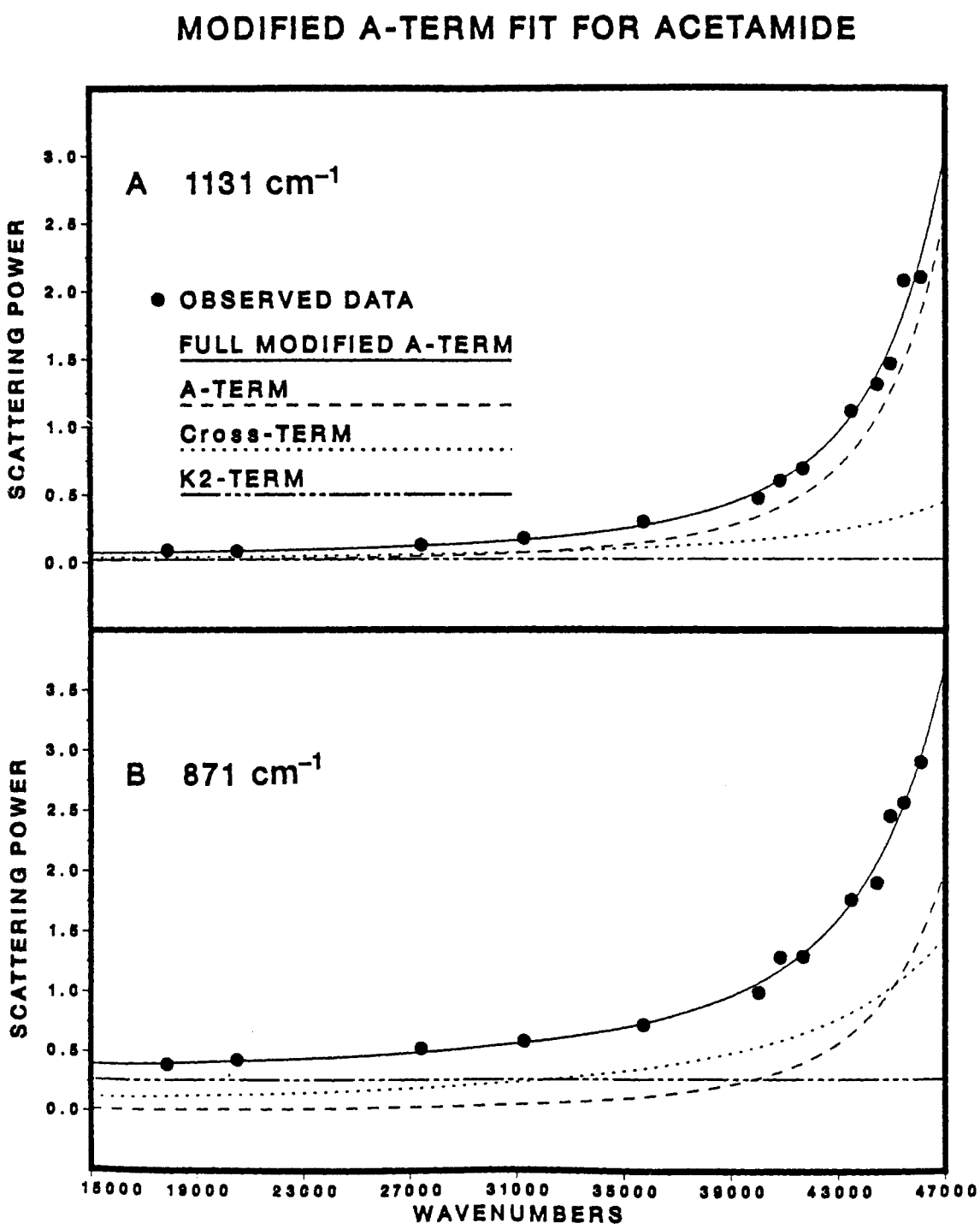

Figure 9. Illustration of the contribution to the Raman scattering strength of the three terms in the square of eq 5: (A) for the acetamide 1131-cm^{-1} band and (B) for the acetamide 871-cm^{-1} band.

higher energy such as $\sigma \rightarrow \sigma^*$ transitions. Similar phenomena were observed for the C–C and C≡N stretches of CH_3CN.[17] The C–C stretch showed much less preresonance enhancement than the C≡N stretch; the A-term transition energy for the C≡N stretch was 116 000 cm^{-1} (86 nm) while it was 39 000 cm^{-1} (26 nm) for the 918-cm^{-1} C–C stretch.

Domination of the preresonance Raman intensities by a single electronic transition has now been observed for acetamide, *N*-methylacetamide, and NO_3^-. In contrast, no single transition appears to dominate the UV preresonance enhancement of acetone, SO_4^{2-}, ClO_4^-, CH_3CN, or the *near*-UV or visible wavelength Raman intensities of benzene.[18] For these species the A-term fits are relatively poor, and the transition energies are unreasonably high, which further indicates that no single state dominates the preresonance enhancement. Indeed, in acetamide and *N*-methylacetamide we see that particular vibrations (those with major C–C stretching contributions) derive some enhancement from higher energy states in addition to the $\pi \rightarrow \pi^*$ transition. The degree of enhancement of a vibration by an electronic transition appears to be related to the relative contribution of atomic displacements of the chromophoric group. These correlations could be used to aid in vibrational assignments.

While the high transition energies found for the preresonant excited states estimated by the A term must signal the contribution of additional states, this contribution does not necessarily have to be constructive. Different electronic states can contribute with both positive and negative sign, and thus, destructive interference can occur as observed previously in porphyrins[47] and benzene.[18,48] A major impediment to the analysis of UV preresonance intensities is the lack of information available on vacuum-UV molecular

(47) Friedman, J.; Hochstrasser, R. M. *Chem. Phys. Lett.* **1975**, *32*, 414.
(48) Korenowski, G. M.; Ziegler, L. D.; Albrecht, A. C. *J. Chem. Phys.* **1978**, *68*, 1248.

excited states. Numerous Rydberg states exist in the vacuum UV. The magnitude of the contribution of Rydberg excited states to the Raman intensity is as yet unclear. However, the results of our studies clearly illustrate that strong isolated transitions, such as the $\pi \rightarrow \pi^*$ transitions in acetamide and *N*-methylacetamide, can lead to strong preresonance intensities. Indeed, these vacuum-UV transitions can dominate the visible wavelength Raman intensities, and should give rise to very strong resonance Raman spectra when excited in the vacuum-UV spectral region.

Conclusions

Preresonance Raman studies of acetone, acetamide, and *N*-methylacetamide indicate that no observable enhancement derives from the weak $n \rightarrow \pi^*$ transitions of these species. The acetone carbonyl stretching vibration shows more preresonance enhancement than the C–C stretching vibrations. The major source of enhancement appears to derive from states in the far-UV. The Raman intensities of acetamide and *N*-methylacetamide are dominated by the ca. 180-nm $\pi \rightarrow \pi^*$ transitions. Essentially all of the preresonance Raman intensities of vibrations containing carbonyl stretches or motions of the nitrogen are due to the $\pi \rightarrow \pi^*$ transitions. Vibrations containing C–C stretches show some contribution from states further in the UV. It appears that an assignment of the transitions contributing to preresonance enhancement can be used to examine the atomic motions important in the molecular vibration. Because of the observed large $\pi \rightarrow \pi^*$ preresonance enhancements it appears that resonance excitation directly into the amide $\pi \rightarrow \pi^*$ transition may result in strong selective enhancements of amide vibrations in peptide and protein samples.

Acknowledgment. We gratefully acknowledge support for this work from NIH Grant 1R01GM30741-03. We also gratefully acknowledge Thanh Phung for technical help in these studies and thank Professor B. Hudson for providing a preprint of his work. S. A. Asher is an Established Investigator of the American Heart Association. This work was done during the tenure of an established investigatorship of the American Heart Association and with funds contributed in part by the American Heart Association, Pennsylvania affiliate.

Registry No. $Me_2C(O)$, 67-64-1; $MeC(O)NH_2$, 60-35-5; MeC(O)NHMe, 79-16-3.

On the Structure and Thermochemistry of the van der Waals Molecule $C_6H_6 \cdot HCl$ and Its Photoion $(C_6H_6 \cdot HCl)^+$

E. A. Walters,*† J. R. Grover,* M. G. White, and E. T. Hui†‡

Department of Chemistry, Brookhaven National Laboratory, Upton, New York 11973
(Received: December 26, 1984; In Final Form: May 20, 1985)

The dissociation energy of the van der Waals complex $C_6H_6 \cdot HCl$ was determined to be 4.79 ± 0.12 kcal mol^{-1} by measurement of the difference between the threshold for the dissociative photoionization of the complex and the ionization potential of C_6H_6. This value is compared to potential well depths obtained by analysis of centrifugal distortion constants for the same complex. The photoionization efficiency function for the production of $(C_6H_6 \cdot HCl)^+$ from $C_6H_6 \cdot HCl$ was obtained between 1280 and 1380 Å. A weak threshold for direct ionization at 1357 ± 7 Å (9.14 ± 0.05 eV) leads to a dissociation energy for $(C_6H_6 \cdot HCl)^+$ of 7.3 ± 1.2 kcal mol^{-1}. The shape of the photoionization efficiency function is interpreted in terms of the involvement of the structure of the complex in the dissociation dynamics. Standard heats of formation are reported for $C_6H_6 \cdot HCl$ (−10.4 kcal mol^{-1}) and $(C_6H_6 \cdot HCl)^+$ (204 kcal mol^{-1}).

Introduction

The geometry of the weak complex between benzene and hydrogen chloride is such that the HCl is, on the average, perpendicular to the benzene ring and on the benzene C_6 axis, with the hydrogen atom closer to the ring than the chlorine atom.[1] However, the same spectroscopic data that were used to obtain the geometry give an ambiguous result for the depth of the potential well binding the two constituents together. Alternative analyses of the same data give well depths $\epsilon = 1950$ cm^{-1} [1b] and $\epsilon = 720$ cm^{-1}.[1a]

We report here the results of a photoionization study of this complex in which the dissociation energy is measured directly by a recently developed technique using dissociative photoionization.[2] In addition, the photoionization efficiency (PIE) curve for the production of $(C_6H_6 \cdot HCl)^+$ has been obtained in the vicinity of threshold. These results lead to determinations of the heats of formation of the neutral and ionic complexes and to deductions about the likely involvement of their structures in the dissociation dynamics.

Experimental Section

The experimental apparatus and technique have already been described.[3] Briefly, the apparatus is a photoionization mass spectrometer equipped with a supersonic nozzle source. Ionizing radiation comes from the vacuum-UV storage ring at the National Synchrotron Light Source at Brookhaven National Laboratory. A 0.2-cm-thick LiF window was placed between the monochromator exit slit and the molecular beam in all of the work reported here to eliminate second- and higher-order light from interfering with the measurements at wavelengths longer than 1200 Å. $C_6H_6 \cdot HCl$ clusters were generated by nozzle expansion of gaseous HCl saturated with benzene vapor at 23 °C, made by bubbling

†Permanent Address: Department of Chemistry, University of New Mexico, Albuquerque, NM 87131.
‡Participant in the National Synchrotron Light Source/High Flux Beam Reactor (NSLS/HFBR) Faculty-Student Support Program at Brookhaven National Laboratory.

(1) Read, W. G.; Campbell, E. J.; Henderson, G. *J. Chem. Phys.* **1983**, *78*, 3501. (b) Read, W. G.; Campbell, E. J.; Henderson, G.; Flygare, W. H. *J. Am. Chem. Soc.* **1981**, *103*, 7670.
(2) Grover, J. R.; Walters, E. A.; Newman, J. K.; White, M. G. *J. Am. Chem. Soc.*, in press.
(3) White, M. G.; Grover, J. R. *J. Chem. Phys.* **1983**, *79*, 4124.

0022-3654/85/2089-3814$01.50/0